Dynamic Response and Shock Resistance of Ferromagnetic Micromechanical Magnetometers

Jeffrey K.Yee[1], Henry H. Yang[2], and Jack W. Judy[1]

[1]Electrical Engineering Dept., University of California, Los Angeles
420 Westwood Plaza, Los Angeles, CA 90094-1594, USA
[2]IBM Almaden Research Laboratory, 650 Harry Road, San Jose, CA 95120-6099, USA

***Abstract*— We have designed, fabricated, and tested ferromagnetic micromechanical magnetometers and have characterized their dynamic response and shock resistance. The magnetometer design is similar to a compass consisting of a ferromagnetic plate and a pair of torsion beams. The susceptibility of these MEMS magnetometers to squeeze film damping is analyzed and compared to experimental results. The torsion beam geometry of the magnetometer is such that longer beams can be used to obtain a higher magnetic sensitivity without compromising device shock resistance.**

I. Introduction

Magnetometers have a variety of applications, such as compassing, magnetic anomaly detection, mineral prospecting, and brain function mapping. In general, it is advantageous to have smaller, lower power, cheaper, and more sensitive magnetometers. However, existing magnetometer technologies (Hall effect, flux gate, SQUID, MR, etc.) do not possess the scaling properties to provide advances on all the desired attributes [1].

Microelectromechanical Systems (MEMS) technology can be used to reduce the size of many types of sensors as well as increase their ability to be mass-produced (e.g., pressure sensors and accelerometers). We have used MEMS technology to realize a novel ferromagnetic magnetometer that operates much like a compass [2]. In our device a magnetized ferromagnetic element is attached to a torsional microflexure (Figure 1). When the device is subjected to an external magnetic field, the mechanical equilibrium established between the magnetic torque T_{mag} and the mechanical restoring torque T_{mech} determines the resultant angular deflection of the magnet. Equating the two torques and solving for the angle of rotation ϕ yields $\phi = (M \times H) \cdot V_{mag} / k_{\phi}$. With magnetization M, magnetic field H, volume of the magnet V_{mag} and angular stiffness of the torsional flexure k_{ϕ}.

Although V_{mag} scales down with the volume of the magnet, k_{ϕ} also has a cubic dimensional dependence. Thus the angle of rotation ϕ is independent of the scale of the device [2].

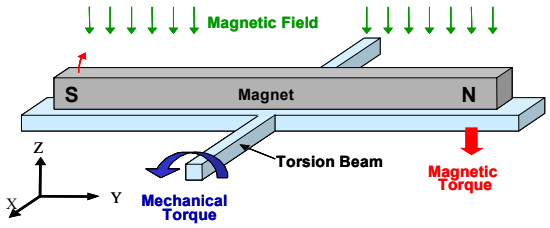

Figure 1. Schematic representation of the ferromagnetic magnetometer.

For this study, we have continued to use the MUMPs foundry process to produce third-generation devices and have integrated a pair of fuses with the magnetometer structure to increase its durability during the release etch as well as during post-release vibration and high-g shock testing. After receiving the MUMPs dies, a 2-mask post-fabrication process is used to selectively electrodeposit the magnet, consisting of CoNi (40%Co, 60%Ni), onto polysilicon plates varying in size (200×100, 600×100, and 1000×100 μm^2). Torsion beams were also varied in length (200, 100, 50, and 25 µm) and width (20, 8, 4 and µm), giving us a total of 30 different magnetometer geometries, each repeated 4 times on a chip (Fig. 2). Using these post-processed dies, we have been able to study the dynamic response and shock resistance of each magnetometer.

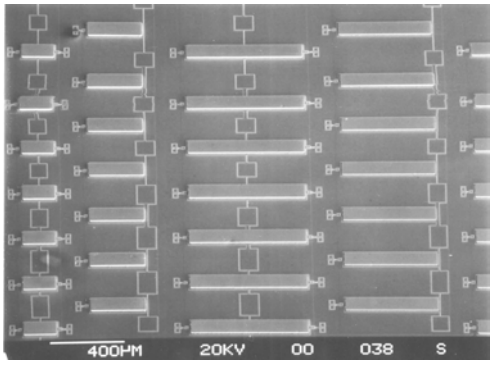

Figure 2. SEM image of some of the MEMS magnetometer geometric permutations.

II. DYNAMIC THEORY AND RESULTS

As is often the case with most MEMS devices, squeeze-film damping tends to limit the performance of MEMS to low frequency ranges. As shown extensively by Senturia and Pan [7-8], modeling of squeeze-film damping entails higher-order mathematics beyond the scope of this paper. In this section, a review of basic squeeze-film damping theory will be presented, followed by the data obtained with our structures.

Squeeze-film damping is most easily understood by modeling the air between a MEMS device and the substrate as both a dampener $b_{squeeze}$ and a spring $k_{squeeze}$ (Fig. 3).

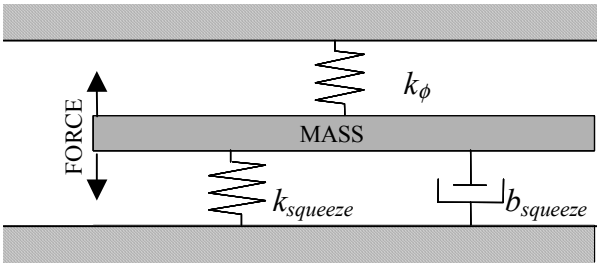

Figure 3. Schematic representation of squeeze-film damping.

At low frequencies the system is overdamped due to viscous damping caused by the $b_{squeeze}$ term; at higher frequencies the damping decreases and the spring effect $k_{squeeze}$ of the gas film dominates [9]. This results in what appears to be a resonance shift. In actuality there exist two resonant frequencies (i.e., one due to $k_{squeeze}$ and one due to k_ϕ), but the overdamping of the lower frequencies damps the natural resonant frequency of the MEMS device and thus the primary resonant peak can not be detected upon measurement. The frequency response of the magnetometers were measured with a laser doppler vibrometer. In our device, the resonant frequency without damping is given by $\omega_0 = (k_\phi / J)^{0.5}$ with angular moment of inertia $J = ml^2/2$ mass m, and length l.

Experimental results showed that although the devices have a theoretical resonant frequency of ~1kHz, the device response rolls-off at a significantly lower frequency (e.g., <100 Hz) and exhibits a resonant peak occurring at a much higher frequency (>20kHz) (Fig. 4).

In order to verify that squeeze film damping was the cause of the faster roll-offs and increased resonant frequencies, devices with differing surface areas as well as devices with etch holes were characterized. From the data in Figure 4, we see that the devices with smaller surface areas and/or etch-holes roll-off more slowly. We also see that as the surface area decreases, the etch holes have a reduced capability of compensating for the squeeze-film damping.

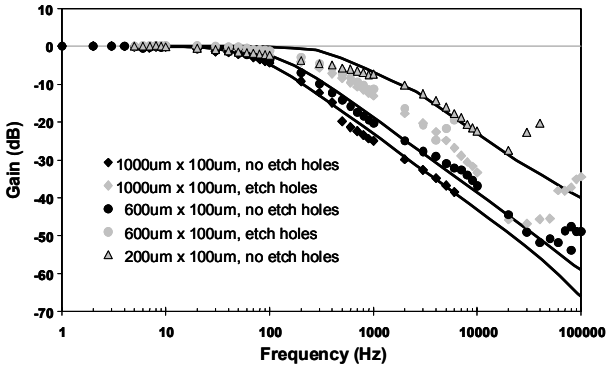

Figure 4. Experimentally measured frequency response of different magnetometer geometries.

III. SHOCK THEORY

For the purpose of analyzing MEMS devices under a shock load, three simplifying assumptions can be made: (i) the package transmits the shock load to the substrate directly (i.e., no damping due to packaging), (ii) when the reference frame is accelerated, the acceleration is transferred to the proof mass through the spring, (iii) devices respond quasi-statically under a shock load [3].

Through these assumptions, classical stress-strain arguments can be applied to the device structure and the magnetometers can be treated as clamped-clamped beams with a point force at the center of the beam. Under normal bending conditions, we find that the stiffness of the clamped-clamped beam is represented by $k_{bending} = 192E \cdot I/(2l)^3$, with elastic modulus E, moment of inertia I, and torsion beam length l [4] (Figure 5a).

Another mode of deformation is that long slender beams act more like a string under tension then a beam bending. Under these conditions the stiffness due to tension is represented by $k_{tension} = 2\sigma \cdot w \cdot t/l$, with stress σ, torsion beam width w, and torsion beam thickness t. (Figure 5b)

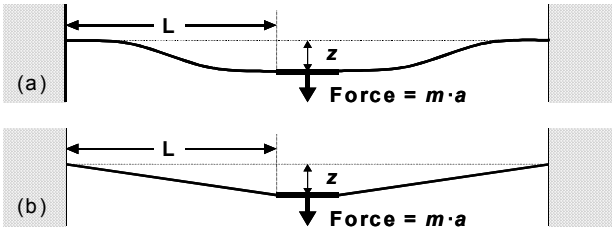

Figure 5. Schematic diagram of clamped-clamped beams in both regimes.

For a given set of torsion beam dimensions, the z-axis displacement, limited by beam bending or tensile loading, can be determined as a function of shock level. Figure 6 plots the z-axis displacement of a long compliant torsion beam and a short stiff torsion beam respectively as a function of shock level. Although tensile forces limit the z-axis displacement of the long slender beam at nearly all levels of shock, bending forces

limit the displacement of the short wide beam except at very high levels of shock (i.e., >10 kG).

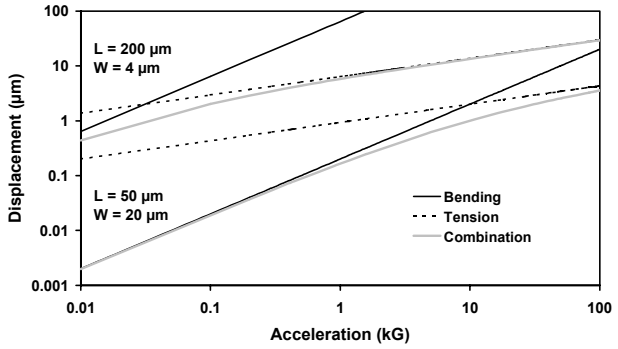

Figure 6. Displacement of a 1000×100×10 µm^3 magnet when suspended by two different beam configurations.

In order to determine the shock resistance of our microstructures we can solve for the acceleration level necessary to reach a given level of fracture strength (e.g., 0.8 to 1.0 GPa for polysilicon) [5-6] for different beam dimensions.

From Figure 7 we can see that short and wide beams require very large shock levels to achieve the fracture stress via bending forces. In Figure 8 it is also clear that very long beams also require a high level of shock to achieve the fracture stress via tensile forces. Surprisingly, 2-µm-thick beams of modest length (e.g., 50 to 100 µm) are the most easily fractured. Experimental results, as shown in the next section, exhibit this same phenomena despite the presence of a large statistical spread.

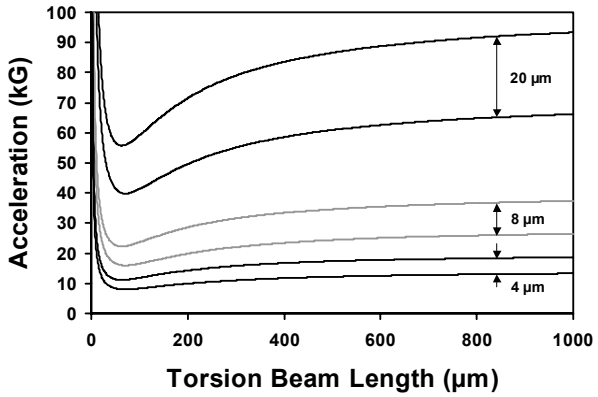

Figure 7. Plot of the acceleration needed to achieve the fracture stress (i.e., 0.8 and 1.0 GPa for the lower and upper lines of each pair) in the torsion beams versus beam length.

IV. Shock Experimental Procedures and Results

A. Preliminary Shock Test

Our initial shock test was performed under "real world" conditions. After mounting the die onto an aluminum substrate with an aluminum protective cover, the package was dropped 25 m onto concrete. While this method is crude, it simulates a "real world" drop, and gives good preliminary data to base more controlled tests. Using classical physics, and an estimation of the deceleration time, we find that the drop generates ~7000 g's.

Some of the observed results were initially surprising. Specifically, all the fuses supporting 1000×100 µm^2 magnetometers fractured and in most cases the torsion bars also broke leaving nothing to retain the magnetic plate to the substrate. However, those magnetometers with the longest and most slender torsion beams (200×4×2 µm^3) survived even though their fuses fractured. These results vividly demonstrate the two different regimes of failure discussed in Section III.

B. Controlled Shock Tests

To further investigate this phenomenon, subsequent testing was done at the Army Research Labs at Aberdeen Proving Grounds in Maryland, USA. Dies were mounted onto 3/8" thick aluminum using Loctite Epoxy E-30CL. These aluminum slabs were then attached to the drop table (Fig. 8). To produce the shock event, the drop table is accelerated downward toward an anvil. Upon contact with the anvil, the drop table decelerates in a matter of microseconds. Figure 9 shows the true acceleration output of a controlled shock test.

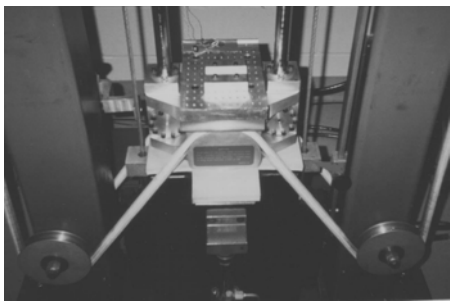

Figure 8. Drop table used to shock test dies. Capable of shocks up to 30,000 g's

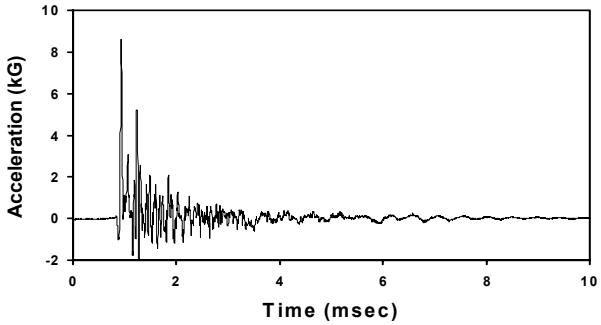

Figure 9. Plot of acceleration vs. time for a typical shock event as measured by an on-board accelerometer

In all tests, the dies remained mounted after even the highest shock level tests (e.g. 10000 G's). A total of six chips were shocked, with varying experimental parameters as listed in table 1.

Table 1. Table of experimental parameters varied for each die.

Die #	Plate Thickness	Fuses	Axis (Fig.1)	Shock (G)
1	10um	Yes	Z	10000
2	10um	Yes	-Z	10000
3	10um	Yes	X	7000
4	10um	Yes	Y	7000
5	10um	No	Z	10000
6	10um	No	Z	5000

Under these controlled conditions, the following results were found:

Z-axis 5,000-G: At 5k-G's no devices were broken or displaced, which correlated well to our expectations.

X&Y-axis 7,000-G: Shocking in the *X* and *Y* directions to a level of 7-kG yielded no substantial loss of structures. The devices have a high rigidity in these directions, which enables them to survive.

Z-axis 10,000-G : Our data on the 4 chips dropped at ~10-kG's, yielded interesting and similar results to the preliminary drop. While our theory states that all large magnetometers should survive a ~10,000 g shock, our statistical results have shown otherwise. Intuitively, the widest and stiffest beams should yield the highest statistical survival rates, which is indeed the case, with both 25×20 and 50×20 μm^2 beams having a survival rate of 56%. While this is of no surprise, the results also show that the most compliant beams (200×4 μm^2 beams) have the same high survival rate, and with a smaller standard deviation.

Table 2. Survival statistics of 600 and 1000 μm plate lengths for 10 kG shocks.

Length (μm)	Width (μm)	Avg	STD
25	4	13%	23%
25	8	28%	33%
25	20	56%	41%
50	4	31%	31%
50	8	34%	31%
50	20	56%	38%
100	4	34%	34%
100	8	34%	31%
100	20	44%	24%
200	4	56%	24%

What this data suggests, is that as beam length increases, survivability due to shock increases as well. Looking at beams shorter than 200 μm and thinner than 20 μm, we see that these beams have a statistically lower survival rate (< 34%). While our theoretical analysis, does indeed predict this phenomena, the collected data has a wide statistical distribution and more data is neeeded with a more complete set of beam lengths and widths, to obtain a more definitive result

V. Conclusion

The frequency response of our magnetometers is significantly impacted by squeeze-film damping. In particular, the frequency response rolls off at lower frequencies and the observable resonant peak shifts to higher frequencies and is reduced in magnitude. The shock resistance of the torsionally suspended microstructures has an intriguing dependence on beam geometry. Specifically,as predicted by theory and observed with our results, beams with either a short and wide configuration or a long and slender configuration had higher survival rates than beams with an in-between geometry. As a consequence, longer beams can be used to obtain more sensitive magnetometers without compromising the shock resistance of the devices.

Acknowledgments

The authors of this paper would like to give a special thanks to T. Gordon Brown and Marshal Childers at Army Research Labs (ARL) for their expertise in shock events and for shock testing our devices. The authors would also like to thank Fardad Chamran, Vishnu Naidu,, the UCLA MAE CAD Lab, UCLA Nanolab, the UCLA Applied MEMS Group, and the UCLA Integrated Photonics Lab.

This work was supported by an NSF Career Award (ECS9876285), DARPA MTO Contract (DABT63-99-1-0020), and NSF XYZ Grant (DMI0089095). The corresponding author is Jack W. Judy. He may be contacted at 68-121 Engineering IV, 420 Westwood Plaza, Los Angeles, CA, 90095-1594, tel: (310) 206-1371, fax: (310) 861-5055, and email: jjudy@ee.ucla.edu. All authors may be contacted via email: Jeff Yee (jeffyee@ee.ucla.edu) and Henry Yang (henryang@us.ibm.com).

References

[1] J. Lenz , "Review of Magnetic Sensors", Proceedings of the IEEE, vol. 78, no. 6, pp. 973-989, June 1990

[2] H. Yang, et al, "Ferromagnetic Micromechanical Magnetometer," Transducers 2001, Munich, Ger., June 2001, pp.164-167

[3] V.T. Srikar and S.D. Senturia, "The Design and Analysis of Shock Resistant Microsystems (MEMS)," Transducers 2001, Munic Ger., June 2001, pp 1370-1373.

[4] W. Young, "Roark's Formulas for Stress and Strain," McGraw-Hill Inc., 1989

[5] Properties of Crystalline Silicon No.20 Edited Robert Hull, INSPEC, IEEE 1999

[6] W. Sharpe Jr., K.M. Jackson, K.J. Hemker, and Z. Xie, "Effect of Specimen Size on Young's Modulus and Fracture Strength of Polysilicon," JMEMS Vol 10, No. 3, Sept 2001, pp 317-326

[7] Y.-J. Yang and S. D. Senturia, "Numerical Simulation of Compressible Squeezed-Film Damping," Tech. Digest, Solid State Sensor and Actuator Workshop Hilton Head Island, SC, June 1996, pp. 76-79.

[8] F. Pan et al. "Squeeze film damping effect on the dynamic response of a MEMS torsion mirror," JMEMS Vol 8 (1998) pp 200-208

[9] Y.-J. Yang, M. Gretillat and S. Senturia, "Effect of Air Damping on the Dynamics of Nonuniform Deformations of Microstructures", Transducers' 1997, Chicago, June 1997.